Volume 11
Number 12
28 March 2023
Pages 2541–2792

Journal of Materials Chemistry B

Materials for biology and medicine

rsc.li/materials-b

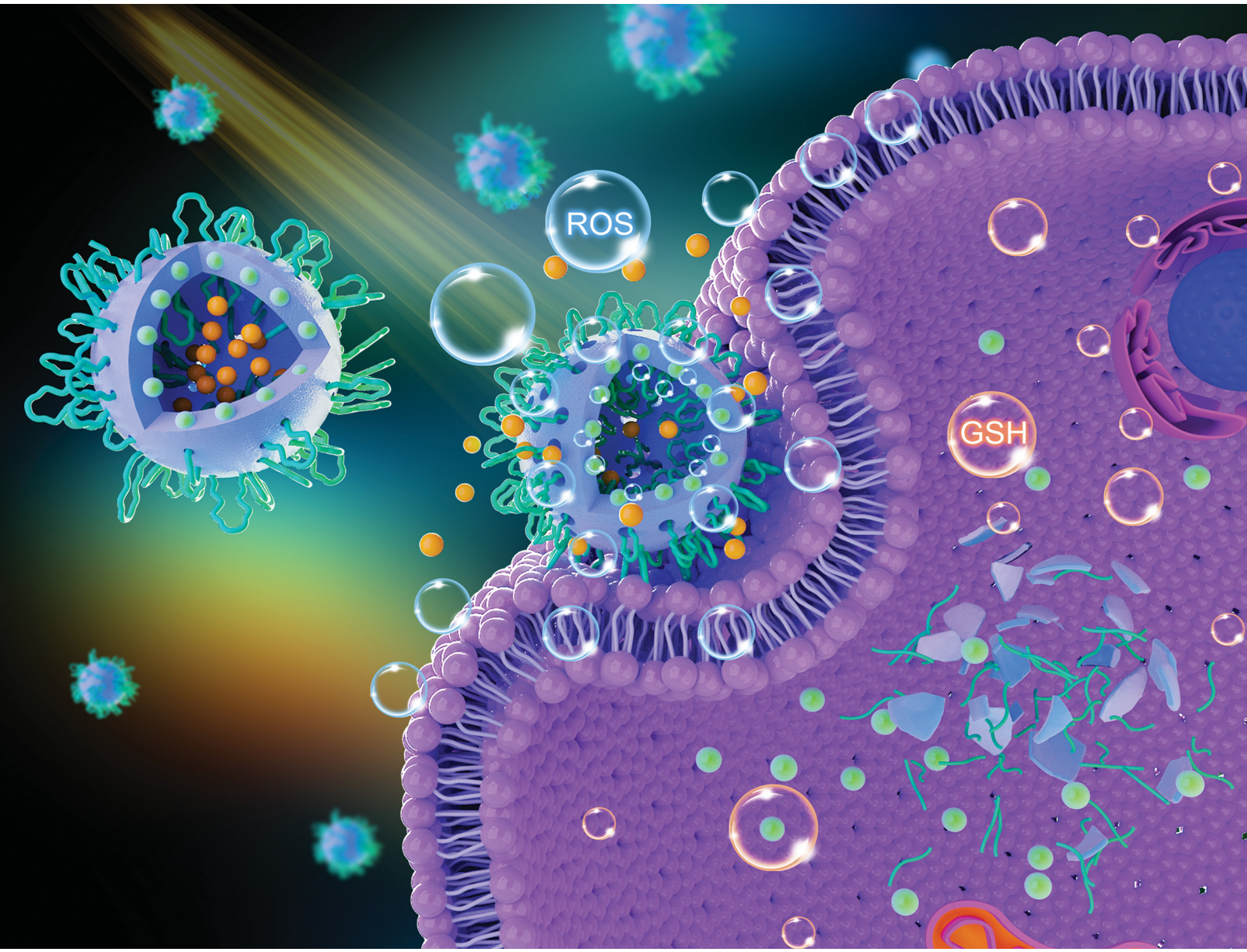

ISSN 2050-750X

ROYAL SOCIETY OF CHEMISTRY

COMMUNICATION

Xiaohong Yin, Mingming Ding *et al.*

Redox-dual-sensitive multiblock copolymer vesicles with disulfide-enabled sequential drug delivery

10 YEARS ANNIVERSARY

Journal of Materials Chemistry B

ROYAL SOCIETY OF CHEMISTRY

COMMUNICATION

View Article Online
View Journal | View Issue

Cite this: J. Mater. Chem. B, 2023, 11, 2631

Received 9th December 2022,
Accepted 3rd February 2023

DOI: 10.1039/d2tb02686d

rsc.li/materials-b

Redox-dual-sensitive multiblock copolymer vesicles with disulfide-enabled sequential drug delivery†

Cheng Cheng,‡[ab] Jiayun Ma,‡[ab] Jinling Zhao,[b] Haiying Lu,[a] Yang Liu,[b] Chuanshi He,[c] Man Lu,[c] Xiaohong Yin,*[a] Jianshu Li [b] and Mingming Ding *[b]

Based on disulfide-enriched multiblock copolymer vesicles, we present a straightforward sequential drug delivery system with dual-redox response that releases hydrophilic doxorubicin hydrochloride (DOX·HCl) and hydrophobic paclitaxel (PTX) under oxidative and reductive conditions, respectively. When compared to concurrent therapeutic delivery, the spatiotemporal control of drug release allows for an improved combination antitumor effect. The simple and smart nanocarrier has promising applications in the field of cancer therapy.

[a] *Science and Technology Innovation Center, Guangyuan Central Hospital, Guangyuan 628000, China*
[b] *College of Polymer Science and Engineering, State Key Laboratory of Polymer Materials Engineering, Sichuan University, Chengdu 610065, China*
[c] *Department of Ultrasound Medical Center, Sichuan Cancer Hospital and Institute, Sichuan Cancer Center, School of Medicine, University of Electronic Science and Technology of China, Chengdu, China*

† Electronic supplementary information (ESI) available. See DOI: https://doi.org/10.1039/d2tb02686d

‡ These authors contributed equally to this work.

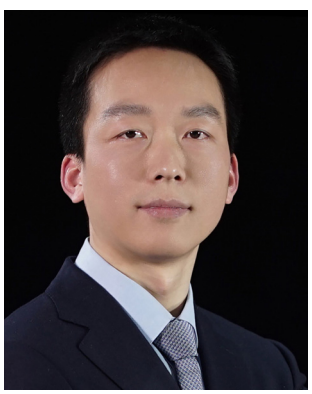

Mingming Ding

Mingming Ding received his BS degree in Polymer Material and Engineering and PhD degree in Materials Science from Sichuan University. After postdoctoral research at Sichuan University, he became an associate professor and professor at College of Polymer Science and Engineering in Sichuan University. His research interests include synthesis and hierarchical self-assembly of biomedical polymers for biomimicry, biosensing and controlled delivery applications.

Cancer remains one of the most devastating diseases that threatens human life. Besides surgery and radiotherapy, a large variety of chemotherapeutic agents have been used in the clinic to effectively treat different types of cancers by targeting specific pathways.[1–8] As single-agent therapies directed to individual targets show limited clinical outcomes due to tumor heterogeneity and drug resistance, combination therapy by co-delivering multiple drugs with different action sites can potentially achieve a synergistic therapeutic effect.[9,10] The advantages of combination therapy include enhanced drug potency against tumor cells, decreased frequency and dosage of drug administration, and minimized toxicity and drug resistance.[11–13] Nonetheless, conventional "cocktail"-based administration of multiple drugs may increase short-time drug exposure in patients and result in severe side effects. Recently, it has been shown that the sequence dependency of some drug combinations played a significant role in chemotherapy, where the pretreated therapeutics make the cancer cells more vulnerable to the post-treatment drugs.[14] Hence, it is anticipated that the clinical benefits of combinational therapy can be maximized by spatiotemporally controlled drug delivery using suitable carriers.

Nanoscale delivery systems provide great possibility for targeted delivery of multiple drugs because of their small sizes, unique surface properties, and structural and functional tunability.[15–21] There are mainly two approaches to the design of nanomaterials for sequential drug release. One is the combination of slow- and quick-release strategies characterized by a rapid release of some drugs and a sustained slow release of others. The release of the drug combination can be controlled through carriers with special structures such as mesoporous silica nanoparticles (MSNs),[22] nanogel-incorporated hydrogel,[23] degradable multilayer fibers,[24] liposomes with dual hydrophobic-hydrophilic depots,[25] *etc.* Another method is the double quick-release strategy, generally triggered by the responses of multiple labile moieties to different stimulation conditions.[26] Despite these advancements, current approaches

to sequential drug delivery still suffer from the incomplete release of post-treatment drugs, requirement of multiple responsive groups, and relatively complex structures of nanomaterials or devices. To date, the development of nanocarriers delivering multiple therapeutics in a predictable and sequentially controllable fashion by a simple method remains a great challenge.

Herein, we report a facile redox potential-controlled sequential delivery of hydrophilic and hydrophobic drugs using a model multiblock copolymer vesicle containing a disulfide bond as the only kind of responsive linkage. It is known that the reactive oxygen species (ROS) concentrations (0.1–1 mM) in the extracellular matrix of tumor tissues are 10–100 times higher than those in the tumor cells, and the intracellular glutathione (GSH) level (10 mM) is much higher than that outside the cells (2–20 μM).[27–31] We envision that the uniquely heterogeneous redox potential would enable spatiotemporal control over drug release by using labile moieties that respond to both ROS and GSH. Therefore, we constructed a polymersome with a disulfide-enriched interlayer *via* segmentation-mediated self-assembly (SDSA),[32] which could accommodate hydrophilic guests in the interior and hydrophobic agents in the membrane (Scheme 1). Specifically, the drug-loaded polymeric vesicles showed oxidative responsiveness under ROS stimulation, achieving the first release of hydrophilic drugs. Besides, the transition of the disulfide bond to sulfoxide or sulphone changed the hydrophobicity and bond energy of the linkage, which made it more sensitive to intracellular GSH to realize the second superfast release of hydrophobic drugs. In addition, the combination of exogenous oxidative stimulation not only accelerated the change of vesicle permeability but also achieved the synergy of chemotherapy, phototherapy and immunogenic cell death (ICD) for improved antitumor effect.

To construct the multiblock copolymer (MCP), polyethylene glycol (PEG, MW 2000) and polycaprolactone (PCL, MW 2000) were coupled with an L-cystine dimethyl ester diisocyanate (CDI) according to a previous report.[32] The successful synthesis of MCP was confirmed by ^{1}H-nuclear magnetic resonance (^{1}H NMR) spectra, where the characteristic peaks of PEG, PCL and CDI residues were observed (Fig. S1, ESI†). The gel permeation chromatography (GPC) diagram indicates a unimodal molecular weight distribution (Fig. S2, ESI†). The multiblock copolymer can form unique flower-like vesicles with a cystine-gathered interlayer *via* SDSA, driven by the interesting interaction and phase separation among multiple PCL and PEG segments (Fig. 1A and B).[32] The particle size was 191 nm with narrow size distribution (PDI = 0.199) (Fig. S3, ESI†), as determined by dynamic light scattering (DLS). To further explore the morphology, we examined the ability of the assemblies to accommodate hydrophilic doxorubicin hydrochloride (DOX·HCl). The fluorescence spectra show that the DOX·HCl-loaded assemblies were quenched compared with the same concentration of DOX·HCl dissolved in an aqueous solution (Fig. 1C), suggesting that the dyes were encapsulated into the hydrophilic cavity of the self-assemblies. A similar quenching effect was also observed when rhodamine 6G (R6G) was loaded into the assemblies (Fig. S4, ESI†). The above results proved the formation of vesicles by MCP.[33–36] To further demonstrate the morphology, the radii of gyration (R_g) and the mean hydrodynamic radii (R_h) were determined by static light scattering

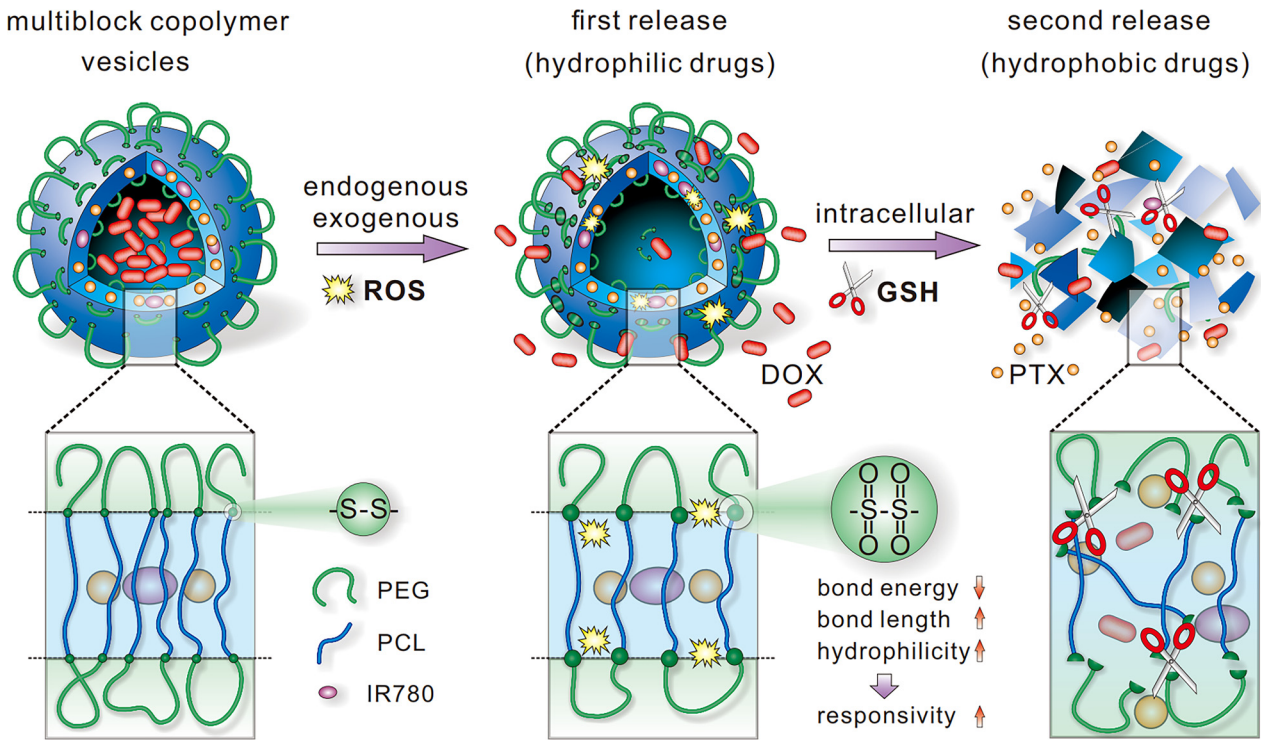

Scheme 1 Schematic illustration of disulfide-enriched multiblock copolymer vesicles toward redox-controlled sequential drug delivery.

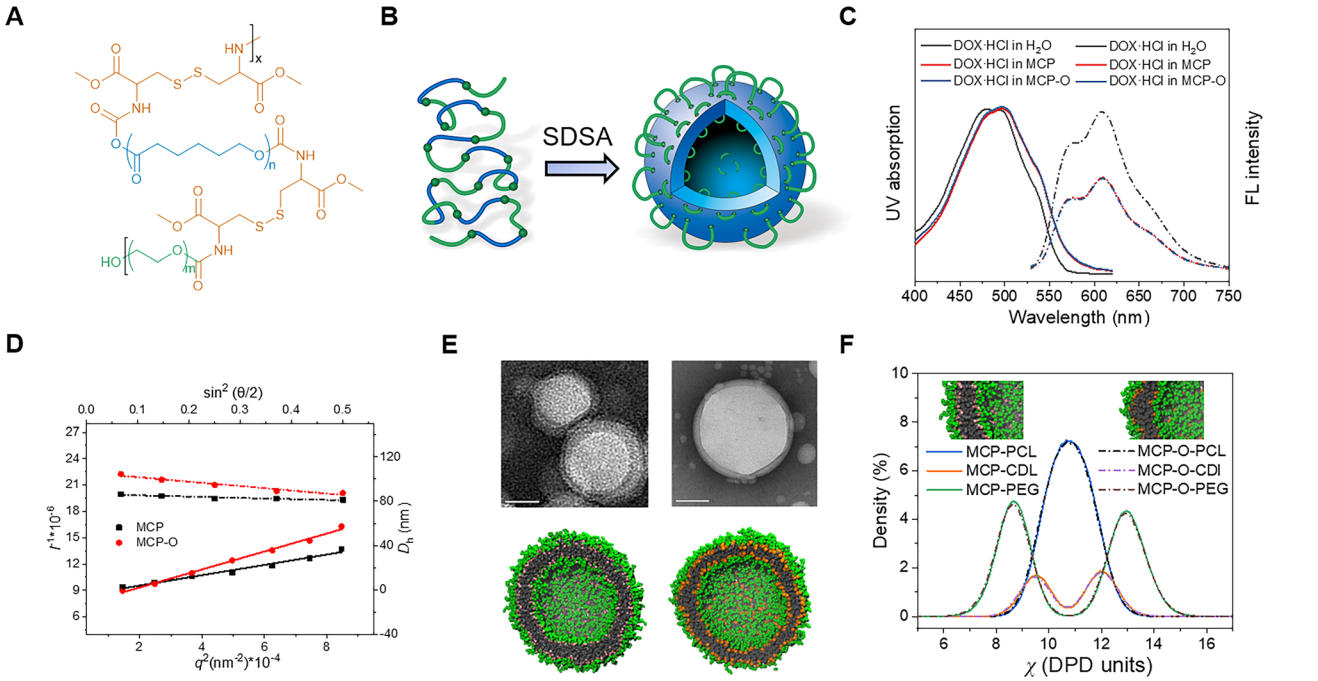

Fig. 1 Schematic illustration of MCP (A) and assemblies (B). (C) UV-vis spectra (left) and fluorescence emission spectra (λ_{ex} = 480 nm, right) of DOX·HCl in H_2O, MCP and MCP-O assemblies. (D) Hydrodynamic diameter associated functions at different incident angles determined by DLS (dotted line) and typical Berry plots using multiangle SLS (solid line) of MCP (square) and MCP-O (circle) assemblies measured at 25 °C. (E) TEM images of MCP (left) and MCP-O assemblies (right). Scale bars: 100 nm. Insets show typical cross-sectional views of MCP (left) and MCP-O assemblies (right). Color code: black, PCL; green, PEG; pink, cystine residues of MCP; yellow, cystine residues of MCP-O. (F) Density profiles of MCP and MCP-O from DPD simulations.

(SLS) and DLS, respectively. The R_g/R_h ratio was calculated to be 1.07, which was strongly indicative of spherical vesicle architecture (Fig. 1D and Table S2, ESI†).[37,38] Transmission electron microscope (TEM) imaging also evidenced that MCP self-assembled into well dispersed and spherical polymersomes (Fig. 1E). To visually investigate the core–shell structure of MCP assemblies, we performed a dissipative particle dynamics (DPD) simulation.[39] The result suggests that MCP can aggregate into a well-defined hollow spherical architecture, where the hydrophobic PCL block formed the membrane, hydrophilic PEG was located in the inner core and outer crown, and cystine residues with disulfide bonds were densely distributed at the hydrophilic/hydrophobic interface (Fig. 1E and F).

The disulfide bond has shown the potential to be oxidized into sulfoxide or sulphone in the presence of ROS.[40] We thus hypothesized that the disulfide-enriched interlayer of MCP vesicles might impart an oxidation-responsive property. To test this hypothesis, the copolymer assemblies were first treated with 500 mM hydrogen peroxide (H_2O_2) and lyophilized for ^{1}H NMR analysis. It was found that the methylene protons near the sulfur atom of MCP were remarkably faded in $CDCl_3$ (Fig. S5, ESI†), owing to the increased polarity of the –S═O groups after oxidation. The GPC diagrams of the oxidized polymer (MCP-O) show a single elution peak without an obvious shift of elution time compared with MCP (Fig. S2, ESI†), revealing that no molecular chain breakage occurred during the oxidation process. Moreover, the new absorption band at ~1150 cm^{-1} in the Fourier transform infrared (FTIR) spectrum of MCP-O was assigned to the symmetric O═S═O stretch vibrations, implying that the thioether groups have been successfully oxidized into sulfone groups (Fig. S6, ESI†). To further estimate the degree of oxidation, we carried out X-ray photoelectron spectroscopy (XPS) experiments. Obviously, the peak assigned to thioether groups (163.08 eV) was declined, while those corresponding to sulfone (167.59 eV) appeared, with a degree of oxidation up to 88.5%. (Fig. S7, ESI†). To investigate whether oxidation impacted the self-assembly behavior, the polymersomes before and after H_2O_2 treatment were measured with DLS. It was found that the particle size increased slightly after oxidation (Fig. S3, ESI†), possibly due to the presence of more hydrophilic sulfoxide or sulphone moieties. Interestingly, unlike previous findings that polymeric nanoparticles were disassociated with the oxidation of thioether groups,[41] the MCP assemblies maintained the vesicular structure after oxidative treatment, as confirmed by DOX·HCl/R6G encapsulation (Fig. 1C and Fig. S4, ESI†), SLS/DLS (Fig. 1D and Table S2, ESI†) and TEM results (Fig. 1E), owing to the fact that oxidation of MCP neither disrupted the molecular chain nor destroyed the amphipathy essential for self-assembly. In addition, DPD simulation verified the vesicle structure of MCP-O with sulphone groups distributed mainly in the interlayer (Fig. 1E and F).

To determine whether the oxidation of disulfide-enriched interlayer of polymersomes enabled controlled drug release, we first loaded DOX·HCl into the vesicles as a hydrophilic drug model. For comparison, we also prepared polymersomes from a

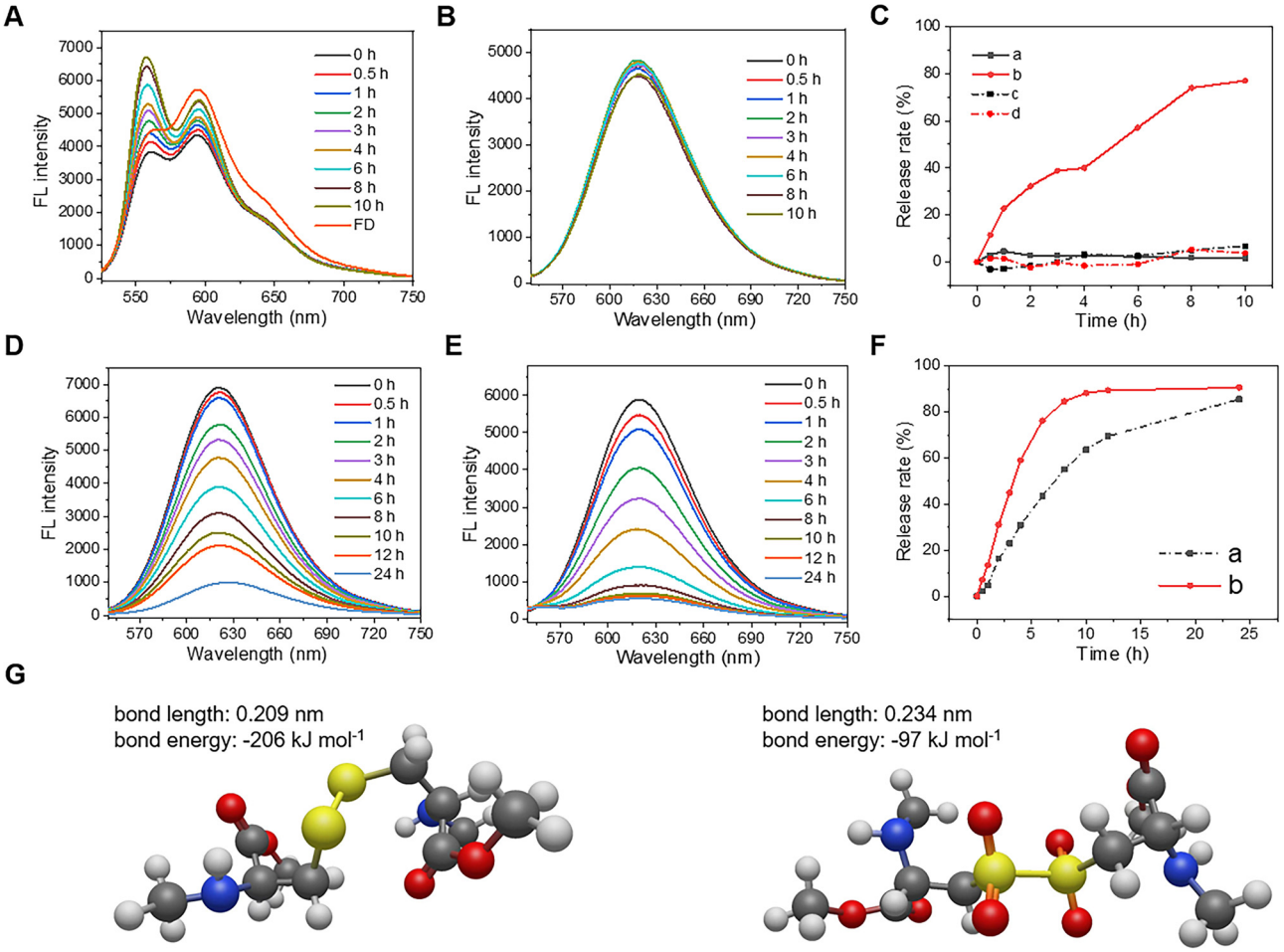

Fig. 2 Fluorescence spectra of MCP vesicles encapsulating DOX·HCl (A) and NR (B) with 500 mM H_2O_2 treatment for different times. FD represents free DOX·HCl in an aqueous solution, with the same concentration of that encapsulated in vesicles. (C) Time-dependent release rates of DOX·HCl (a and b) and NR (c and d) from MCP assemblies incubated with H_2O (a and c) and H_2O_2 (b and d). Fluorescence spectra of NR-encapsulated MCP (D) and MCP-O (E) incubated with 10 mM GSH treatment for different times. (F) Time-dependent release rates of NR from MCP (a) and MCP-O (b). (G) Computational snapshots of the disulfide bonds in MCP (left) and MCP-O (right). Carbon, hydrogen, oxygen, nitrogen and sulfur are rendered in grey, white, red, blue and yellow, respectively.

conventional diblock copolymer containing one disulfide linkage between PCL and PEG segments (DCP) and a lysine-derived multiblock copolymer without a disulfide bond (MLP) according to reports.[32,42] It was found that the DOX·HCl- encapsulated DCP and MLP vesicles did not show a noticeable change in fluorescence upon oxidation treatment (Fig. S8 and S9, ESI†). To our surprise, the dye was gradually released from the MCP nanovehicles under oxidative stimulation, as evidenced by the recovery of DOX·HCl fluorescence over time (Fig. 2A–C). This result indicates that the oxidation of disulfide linkages increased the permeability of MCP vesicles, which may be associated with the formation of unique membrane structures and cystine-gathered interface driven by the phase separation between multiple PCL and PEG blocks.[32] The exact mechanism is unclear and requires further examination. Furthermore, we also used Nile red (NR) as a drug model to study the release of hydrophobic drugs. As expected, the fluorescence intensity of all the NR-loaded vesicles was nearly unchanged in the presence of ROS (Fig. 2B and C), implying that oxidation did not induce the release of hydrophobic payloads. In contrast, the DCP, MCP and MCP-O vesicles encapsulating NR displayed a significant decrease in emission intensity under an intracellular level of GSH (10 mM) (Fig. 2D–F and Fig. S10, ESI†), suggesting that the nanovehicles exhibited good reduction-responsive properties due to the presence of reduction-responsive disulfide linkages as well as their oxidized derivatives. For comparison, the fluorescence spectra of NR-encapsulated MLP without a labile group did not show NR release under GSH stimulation (Fig. S11, ESI†). Interestingly, we found that the release rate of NR from MCP-O vesicles was much higher than that from MCP vesicles (Fig. 2F). There are probably two reasons to account for the enhanced responsivity. One is that oxidation increased the hydrophilicity of the particle interface, thus facilitating the attack of reducing agents.[43] The other is that the oxidized disulfide bonds containing sulfur or sulphone bonds might be more labile and easier to be cleaved by GSH. To validate this hypothesis, we carried out a density functional theory (DFT) calculation to compute and compare the bond energy of

disulfide moieties in MCP and MCP-O copolymers. The targeted components of the two molecules are shown in Fig. 2G. After computation, the bond energies of the disulfide bonds in MCP and MCP-O were found to be −206 and −97 kJ mol^{-1}, and the bond lengths of the two linkages were 0.209 and 0.234 nm, respectively. The decreased bond energy and increased bond length verify a decreased stability of the oxidized disulfide linkages in MCP-O.

The specific release of hydrophilic and hydrophobic payloads under different conditions prompted us to further explore the potential of MCP in sequential drug delivery, in view of the significant redox gradient between extracellular and intracellular microenvironments.[44,45] DOX can bind to DNA or RNA to inhibit the synthesis of nucleic acids, while paclitaxel (PTX) can induce the apoptosis of tumor cells by blocking cell cycle progression in the late G2-M phases.[46] The combination of DOX and PTX has been used as the first-line treatment for metastatic breast cancer,[47] but the sequential delivery of such drug combinations in a single carrier was rarely investigated. We envision that the sequential delivery of the two drugs with different action mechanisms may exhibit better antitumor effect compared to concurrent delivery. To test this conjecture, we treated the GL261 cells with hydrophilic DOX·HCl and hydrophobic PTX concurrently or sequentially. As we expected, the cells incubated with two drugs sequentially showed a lower viability than those treated by the two drugs simultaneously (Fig. S12, ESI†). Thus, DOX·HCl and PTX as a model antitumor drug combination were loaded into the polymersomes. To compensate for the relatively low level of endogenous ROS in the tumor microenvironment, we also introduced a photosensitizer IR780 into the assemblies to supplement exogenous ROS. We have confirmed that the photoactivated nanoreactor enabled laser-controlled generation of singlet oxygen ($^1O_2$) and oxidation of polymersomes *in situ* for efficient release of DOX·HCl, without noticeable leakage of hydrophobic payloads (Fig. S13 and S14, ESI†). Hence, the drug-loaded nanoreactors were incubated with GL261 cells followed by 3 min of NIR irradiation. Fluorescence microscope imaging evidenced an 11.2-fold higher 2′,7′-dichlorofluorescein (DCF) fluorescence in the cells as compared with the non-illuminated group (Fig. 3A and B), confirming the effective generation of ROS from the nanoreactor. Next, the drug efficacy of different formulations towards GL261 cells was visually observed under a fluorescence microscope, wherein the live and dead cells were

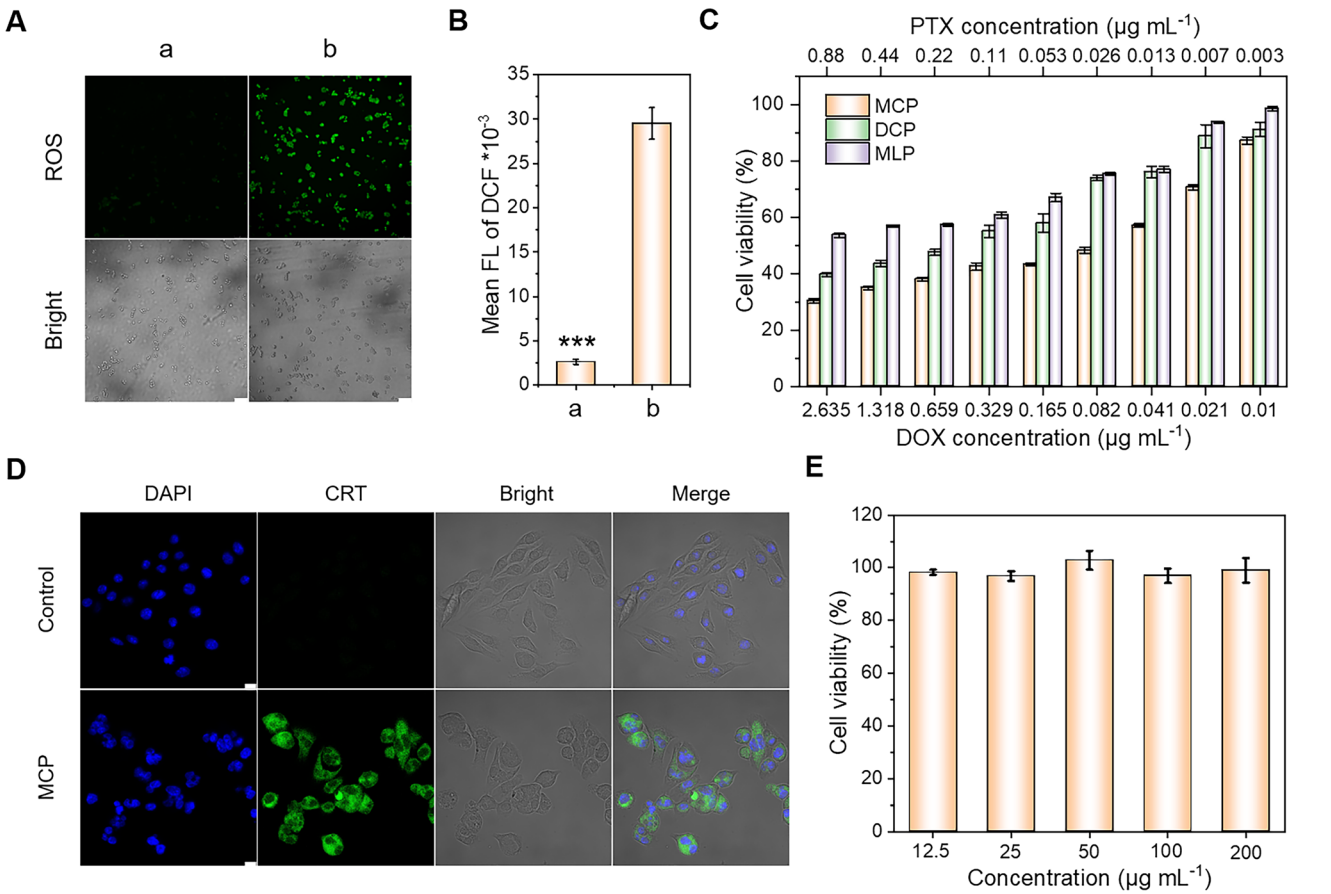

Fig. 3 (A) *In vitro* ROS detection of GL261 cells incubated with drug-loaded nanoreactors with (a) or without (b) NIR irradiation. Scale bars: 50 μm. (B) Semi-quantitative analysis of intracellular DCF fluorescence. (C) Cell viability of GL261 cells incubated for 24 h with drug-loaded nanoreactors at different DOX·HCl and PTX concentrations after irradiation by an 808 nm laser for 3 min. (D) CLSM images of CRT exposure in GL261 cells with the above treatments. Scale bars: 10 μm. (E) Cell viability of 3T3 cells incubated with drug-free MCP at different concentrations for 24 h.

stained with calcein-AM (green) and propidium iodide (PI, red), respectively. It was found that DOX·HCl and PTX co-encapsulated MCP vesicles (sequential release group) exhibited much greater cell death than drug-loaded DCP (concurrent release group) and MLP vesicles (non-responsive group) with the same dosage and duration of light treatment (Fig. S15, ESI†). The half maximal inhibitory concentrations (IC50) of DOX·HCl were 0.16 (MCP), 0.65 (DCP) and 2.01 μg mL^{-1} (MLP) as determined by a cell counting kit-8 (CCK-8) assay (Fig. 3C). The results demonstrate a synergistic therapeutic effect resulted from phototherapy and sequential release of DOX·HCl and PTX. Moreover, the drug-loaded MCP vesicles also promoted evident calreticulin (CRT) expression on the surface of GL261 cell membranes compared with the control group (Fig. 3D), indicating an ICD of tumor cells caused by combinational phototherapy and chemotherapy.[48] In addition, the multiblock copolymers were constructed from PCL, PEG and L-amino acid derivatives and did not show any inhibitory effect against 3T3 cells or GL261 cells (Fig. 3E and Fig. S16 and S17, ESI†), which are inherently biocompatible for use as smart nanocarriers for photo-chemo-immunotherapy of tumors.

Conclusions

In summary, we have developed redox-dual-sensitive multiblock copolymer vesicles *via* segmentation-mediated self-assembly. The nanovessels showed enhanced permeability under oxidative conditions for specific release of hydrophilic drugs, followed by the second release of hydrophobic therapeutics triggered by the intracellular level of GSH. Further combination of IR780 enabled a photoactivated nanoreactor for *in situ* generation of ROS and redox-controlled sequential release of DOX·HCl and PTX for synergistic phototherapy and chemotherapy. Our work provides a simple approach for the design and construction of sequential drug delivery nanoplatforms, which holds great promise for improving the clinical benefits of combinational cancer therapy.

Author contributions

Conceptualization, funding acquisition, resources: M. D. and X. Y.; formal analysis, methodology, visualization, writing - original draft: C. C. and J. M.; data curation, investigation, software: J. Z., H. L. and Y. L.; validation: C. H. and M. L.; project administration, supervision: J. L.; writing - review & editing: all authors.

Conflicts of interest

There are no conflicts to declare.

Acknowledgements

The research was supported by the National Key R&D Program of China (2019YFE0196700), the National Natural Science Foundation of China (51873118, 52022062, 52273140), the Application and Basic Research of Sichuan Department of Science and Technology (2021YJ0225) and the Project of State Key Laboratory of Polymer Materials Engineering.

Notes and references

1 R. Yang, Y. Zheng, X. Shuai, F. Fan, X. He, M. Ding, J. Li, H. Tan and Q. Fu, *Adv. Sci.*, 2020, **7**, 1902701.
2 M. Ding, N. Song, X. He, J. H. Li, L. Zhou, H. Tan, Q. Fu and Q. Gu, *ACS Nano*, 2013, **7**, 1918–1928.
3 M. Ding, J. Li, X. He, N. Song, H. Tan, Y. Zhang, L. Zhou, Q. Gu, H. Deng and Q. Fu, *Adv. Mater.*, 2012, **24**, 3639–3645.
4 J. Wei, X. Shuai, R. Wang, X. He, Y. Li, M. Ding, J. Li, H. Tan and Q. Fu, *Biomaterials*, 2017, **145**, 138–153.
5 L. Huang, J. Liu, F. Gao, Q. Cheng, B. Lu, H. Zheng, H. Xu, P. Xu, X. Zhang and X. Zeng, *J. Mater. Chem. B*, 2018, **6**, 4618–4629.
6 L. Huang, S. Hu, Y. Fu, Y. Wan, G. Li and X. Wang, *J. Mater. Chem. B*, 2022, **6**, 4618–4629.
7 Q. Jin, Y. Deng, X. Chen and J. Ji, *ACS Nano*, 2019, **13**, 954–977.
8 W. Zhang, X. Lyu, L. Zhang, W. Wang, Q. Shen, S. Lu, L. Lu, M. Zhan and X. Hu, *Macromol. Rapid Commun.*, 2022, **43**, 2100918.
9 K. Zhu, J. Hu and S. Liu, *Macromolecules*, 2019, **51**, 8530–8538.
10 R. Bholakant, B. Dong, X. Zhou, X. Huang, C. Zhao, D. Huang, Y. Zhong, H. Qian, W. Chen and J. Feijen, *J. Mater. Chem. B*, 2021, **9**, 8718–8738.
11 S. Gadde, *MedChemComm*, 2015, **6**, 1916–1929.
12 J. Li, Y. Wang, Z. Pei and Y. Pei, *Chem. Commun.*, 2022, **58**, 3338–3341.
13 M. Lu, M. Wu, Y. Huang, J. Yao, Z. Shao and X. Chen, *J. Mater. Chem. B*, 2022, **10**, 3798–3807.
14 S. Song, S. Kim, D. Oh, Y. Lee, A. Lee, Y. Jeong, H. Bae, D. Lee, S. Lee, J. Kim and S. Kwon, *Adv. Sci.*, 2019, **6**, 1801380.
15 M. Ding, J. Li, H. Tan and Q. Fu, *Soft Matter*, 2012, **8**, 5414–5428.
16 C. Zhang, D. Li, P. Pei, W. Wang, B. Chen, Z. Chu, Z. Zha, X. Yang, J. Wang and H. Qian, *Biomaterials*, 2020, **237**, 119835.
17 J. Chen, J. Yang and J. Ding, *J. Mater. Chem. B*, 2022, **10**, 7173–7182.
18 L. Qiao, H. Yang, S. Gao, L. Li, X. Fu and Q. Wei, *J. Mater. Chem. B*, 2022, **10**, 1908–1922.
19 J. Yang, H. Zou, J. Ding and X. Chen, *Acta Polym. Sin.*, 2021, **52**, 960–977.
20 C. Yao, Y. Li, Z. Wang, C. Song, X. Hu and S. Liu, *ACS Nano*, 2020, **14**, 1919–1935.
21 Z. Wang, M. Zhan and X. Hu, *Chem. – Eur. J.*, 2022, **28**, e202200042.
22 Y. Liu, B. Huang, J. Zhu, K. Feng, Y. Yuan and C. Liu, *RSC Adv.*, 2018, **8**, 40598–40610.
23 W. Yang, P. Zhou, L. Liang, Y. Cao, J. Qiao, X. Li, Z. Teng and L. Wang, *ACS Appl. Mater. Interfaces*, 2018, **10**, 18560–18573.

24 X. Li, Y. He, J. Hou, G. Yang and S. Zhou, *Small*, 2020, **16**, 1902262.
25 S. Morton, M. Lee, Z. Deng, E. Dreaden, E. Siouve, K. Shopsowitz, N. Shah, M. Yaffe and P. Hammond, *Sci. Signaling*, 2014, **7**, ra44.
26 Y. Li, W. Li, W. Bao, B. Liu, D. Li, Y. Jiang, W. Wei and F. Ren, *Nanoscale*, 2017, **9**, 9317–9324.
27 Y. Ma, J. Wang, W. Tao, C. Sun, Y. Wang, D. Li, F. Fan, H. Qian and X. Yang, *ACS Appl. Mater. Interfaces*, 2015, **7**, 26315–26325.
28 J. Wu, L. Zhao, X. Xu, N. Bertrand, W. Choi, B. Yameen, J. Shi, V. Shah, M. Mulvale, J. Maclean and O. Farokhzad, *Angew. Chem., Int. Ed.*, 2015, **54**, 9218–9223.
29 K. Zhu, G. Liu, J. Hu and S. Liu, *Biomacromolecules*, 2017, **18**, 2571–2582.
30 J. Ding, J. Chen, D. Li, C. Xiao, J. Zhang, C. He, X. Zhuang and X. Chen, *J. Mater. Chem. B*, 2013, **1**, 69–81.
31 H. Han, H. Wang, Y. Chen, Z. Li, Y. Wang, Q. Jin and J. Ji, *Nanoscale*, 2016, **8**, 283–291.
32 Y. Zheng, C. Weng, C. Cheng, J. Zhao, R. Yang, Q. Zhang, M. Ding, H. Tan and Q. Fu, *Macromolecules*, 2020, **53**, 5992–6001.
33 H. Liu, R. Wang, J. Wei, C. Cheng, Y. Zheng, Y. Pan, X. He, M. Ding, H. Tan and Q. Fu, *J. Am. Chem. Soc.*, 2018, **140**, 6604–6610.
34 Z. Li, Y. Yang, C. Peng, H. Liu, R. Yang, Y. Zheng, L. Cai, H. Tan, Q. Fu and M. Ding, *Chin. Chem. Lett.*, 2021, **32**, 1563–1566.
35 Y. Zhou, F. Fan, J. Zhao, Z. Wang, R. Wang, Y. Zheng, H. Liu, C. Peng, J. Li, H. Tan, Q. Fu and M. Ding, *Nat. Commun.*, 2022, **13**, 4551.
36 H. Liu, Y. Zhou, Y. Liu, Z. Wang, Y. Zheng, C. Peng, M. Tian, Q. Zhang, J. Li, H. Tan, Q. Fu and M. Ding, *Angew. Chem., Int. Ed.*, 2022, e202213000.
37 Y. Zheng, Z. Wang, Z. Li, H. Liu, J. Wei, C. Peng, Y. Zhou, J. Li, Q. Fu, H. Tan and M. Ding, *Angew. Chem., Int. Ed.*, 2021, **60**, 22529–22536.
38 C. Weng, H. Chen, T. Xu, Z. Li, X. Liu, M. Ding, Q. Zhang, H. Tan and Q. Fu, *ACS Mater. Lett.*, 2020, **2**, 602–609.
39 M. Ding, X. He, Z. Wang, J. Li, H. Tan, H. Deng, Q. Fu and Q. Gu, *Biomaterials*, 2011, **32**, 9515–9524.
40 B. Sun, C. Luo, H. Yu, X. Zhang, Q. Chen, W. Yang, M. Wang, Q. Kan, H. Zhang, Y. Wang, Z. He and J. Sun, *Nano Lett.*, 2018, **18**, 3643–3650.
41 T. Deming, *Bioconjugate Chem.*, 2017, **28**, 691–700.
42 G. Lin, L. Cosimbescu, N. Karin, A. Gutowska and B. Tarasevich, *J. Mater. Chem. B*, 2013, **1**, 1249–1255.
43 C. Tian, J. Guo, Y. Miao, S. Zheng, B. Sun, M. Sun, Q. Ye, W. Liu, S. Zhou, K. Kamei, Z. He and J. Sun, *J. Med. Chem.*, 2021, **64**, 15936–15948.
44 Y. Li, S. Lv, Z. Song, J. Dang, X. Li, H. He, X. Xu, Z. Zhou and L. Yin, *Nanoscale*, 2018, **10**, 14554–14562.
45 J. Zhang, Y. Lin, Z. Lin, Q. Wei, J. Qian, R. Ruan, X. Jiang, L. Hou, J. Song, J. Ding and H. Yang, *Adv. Sci.*, 2022, **9**, 2103444.
46 S. Lv, Z. Tang, M. Li, J. Lin, W. Song, H. Liu, Y. Huang, Y. Zhang and X. Chen, *Biomaterials*, 2014, **35**, 6118–6129.
47 W. Chen, G. Luo and X. Zhang, *Adv. Mater.*, 2019, **31**, 1802725.
48 S. Chen, D. Li, X. Du, X. He, M. Huang, Y. Wang, X. Yang and J. Wang, *Nano Today*, 2020, **35**, 100924.